Low-p_T collective flow induces high-p_T jet quenching

Néstor Armesto, Carlos A. Salgado, and Urs Achim Wiedemann

Department of Physics, CERN, Theory Division, CH-1211 Genève 23, Switzerland

(Received 23 March 2005; published 30 December 2005)

Data on low-p_T hadronic spectra are widely regarded as evidence of a hydrodynamic expansion in nucleus-nucleus collisions. In this interpretation, different hadron species emerge from a common medium that has built up a strong collective velocity field. Here we show that the existence of a collective flow field implies characteristic modifications of high-p_T parton fragmentation. We generalize the formalism of parton energy loss to the case of flow-induced oriented momentum transfer. We also discuss how to embed this calculation in hydrodynamic simulations. Flow effects are found to result generically in characteristic asymmetries in the $\eta \times \phi$ plane of jet-energy distributions and of multiplicity distributions associated with high-p_T trigger particles. However, collective flow also contributes to the medium-induced suppression of single inclusive high-p_T hadron spectra. In particular, we find that low-p_T elliptic flow can induce a sizable additional contribution to the high-p_T azimuthal asymmetry by selective elimination of those hard partons that propagate with significant inclination against the flow field. This reduces, at least partially, the recently observed problem that models of parton energy loss tend to underpredict the large azimuthal asymmetry v_2 of high-p_T hadronic spectra in semiperipheral Au + Au collisions.

I. INTRODUCTION

What happens if a hard process, such as the production of high-E_T jets, is embedded in a dense nuclear environment created, e.g., in a nucleus-nucleus collision at the Brookhaven National Laboratory's Relativistic Heavy Ion Collider (RHIC) or at the Large Hadron Collider (LHC) ? While parton-parton interactions at high virtuality $Q^2 \gg \Lambda_{QCD}^2$ occur at too-short time and length scales to be affected by the typical modes in the medium, the parton showers associated with the incoming and outgoing state can interact with the medium [1–6]. This is expected to result in an energy degradation of the leading parton [1–6], in a transverse momentum broadening of the parton shower [7–10], and in an enhanced and softened multiplicity distribution of the hadronic final state [10]. Measurements in Au + Au collisions at the RHIC support this picture by the observed suppression of leading hadron spectra [11–16] and leading back-to-back correlations [17], as well as the medium-modified "jetlike" properties of particle production associated with high-p_T trigger particles [18–20]. The analysis of these "jet-quenching" observables has become one of the most active and most diverse research fields in ultrarelativistic nucleus-nucleus collisions, mainly because the pattern of medium-induced partonic energy loss is expected to allow for a detailed characterization of the properties of the produced dense medium.

Parton energy loss is known to be sensitive to the total in-medium path length and to the average squared transverse momentum transferred from the medium to the hard parton [21–25]. In recent phenomenological studies, the latter quantity has been parametrized by the Baier-Dokshitzer-Mueller-Peigné-Schiff (BDMPS) transport coefficient $\hat{q}$ [10,26] or by physically equivalent model-dependent quantities such as twist-4 multiple-scattering matrix elements [27], the medium opacity, or the number of initially produced gluons per unit rapidity [28]. These model parameters can be related to the

energy density of the produced matter [10,29,30]:

$$\hat{q}(\xi) = c\epsilon^{3/4}(\xi). \tag{1.1}$$

Here, c is a medium-dependent constant ($c \sim 2$ for the case of an ideal quark-gluon plasma [26,29]), and Eq. (1.1) also holds for a time-dependent energy density, as indicated by the explicit ξ dependence. Recently, several phenomenological analyses have used the medium modifications of high-p_T hadron production to extract information about the energy density attained in nucleus-nucleus collisions at the RHIC [24,26,27,31]. These models also account successfully for the centrality dependence of the suppression pattern [27,31,32] and the reduction of leading back-to-back correlation [27,31,32]. However, they tend to underpredict [31,32] the elliptic flow $v_2(p_T)$ at high transverse momentum, which is thought to originate from parton energy loss in an azimuthally asymmetric geometry [28,33].

In nucleus-nucleus collisions at the RHIC and at the CERN Super Proton Synchrotron (SPS), there is strong experimental evidence that the produced medium is only *locally*—-if at all—equilibrated and is thus characterized only *locally* by its energy density. Measurements of low-p_T inclusive hadron spectra [34, 35] and their azimuthal asymmetry [36–38] support the picture that different hadron species emerge from a common medium that has built up a strong collective velocity field [39–43]. These measurements are broadly consistent with calculations based on ideal hydrodynamics [41–45], in which the dynamic behavior of the produced QCD matter is fully specified by its equation of state $p = p(\epsilon, T, \mu_B)$ that enters the energy-momentum tensor

$$T^{\mu\nu}(x) = (\epsilon + p)u^\mu u^\nu - pg^{\mu\nu}. \tag{1.2}$$

For the case of a longitudinal Bjorken-type flow field $u^\mu = (1, \vec{\beta})/\sqrt{1 - \beta^2}, \vec{\beta} = \beta\hat{z}$, the longitudinal component of the energy-momentum tensor increases from $T^{zz} = p$ to
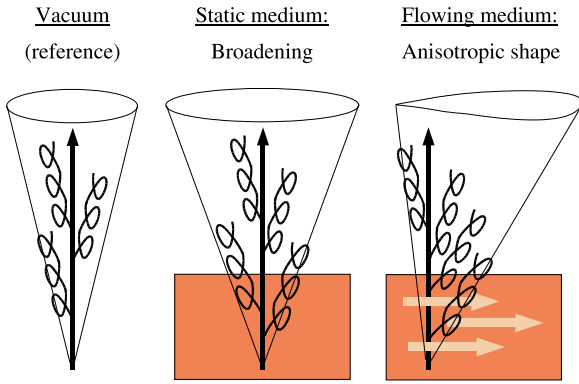
FIG. 1. (Color online) Sketch of the expected energy or multiplicity distribution of a jet fragmenting (left) in the vacuum (middle) in a medium that is longitudinally comoving with the rest frame of the jet, and (right) in a medium that is longitudinally boosted with respect to the rest frame of the jet.

$T^{zz} = p + \Delta p$, where $\Delta p = (\epsilon + p)u^z u^z = 4p\beta^2/(1 - \beta^2)$ for the equation of state of an ideal gas, $\epsilon = 3p$. For a rapidity difference $\eta = 0.5, 1.0,$ and 1.5 between the rest frame that is longitudinally comoving with the jet and the rest frame of the medium, the component T^{zz} of the energy-momentum tensor "seen" by the hard parton is thus increased by a factor of 1, 5, and 18, respectively. It is thus reasonable to assume that the momentum transfer from the medium to a test particle such as a hard parton does not depend solely on the local energy density ϵ, but rather on the energy-momentum tensor (1.2), which involves a significant directed collective flow field $u_\mu(x)$ [46].

Figure 1 sketches the qualitative picture first advocated in Ref. [46]: A jet that fragments inside a medium is known to broaden its shape and to soften its multiplicity distribution. However, if the medium exhibits a collective motion, then a smaller local energy density is sufficient for the same net momentum transfer to the hard parton and thus for the same medium-induced parton energy loss. Moreover, the directed momentum transfer can be expected to break the rotational symmetry of the jet shape in the $\eta \times \phi$ plane. In this work, we give a detailed description of the formalism incorporating these effects and we explore observable consequences of the resulting interplay of oriented and random momentum transfer to a hard parton.

For each jet, rotational symmetry in the $\eta \times \phi$ plane is broken even in the absence of a medium, mainly for two reasons: Statistically, any finite multiplicity distribution of a rotationally symmetric sample breaks the rotational symmetry. If this were the only source of symmetry breaking, one could search for medium-induced asymmetries in realigned jet samples, similar to the analysis of elliptic flow in realigned event samples [47,48]. In addition, however, the k_T ordering of the Dokshitzer-Gribov-Lipatov-Altarelli-Parisi (DGLAP) parton shower implies that the first parton splitting in the shower contains significantly more transverse momentum than the second, thus leading to a dynamical asymmetry in the $\eta \times \phi$ plane. Both effects lead to symmetry breaking in a *random* direction in the $\eta \times \phi$ plane—thus rotational symmetry is restored in sufficiently large jet samples. To search for symmetry-breaking effects caused by collective motion in $\eta \times \phi$ distributions of jet energy and jet multiplicity, it is thus important to control experimentally the direction of this collective motion. From these arguments, we foresee two classes of applications for our calculations.

First, in general, a hard parton needs not be produced in the Lorentz frame that is longitudinally comoving with the medium (Fig. 2a); and even if it is produced in the longitudinally comoving frame, it will in general not stay in this frame during the entire time evolution of the medium. This is so because the hard parton moves—like any effectively massless particle—on a straight lightlike line in the (z, t) diagram, whereas the collective flow field is expected to show significant deviations [49,50] from Bjorken expansion and will thus intersect this straight line. In such cases, the collective component of the momentum transfer to the hard parton is directed along the beam axis. Hence averaged samples of medium-modified jet shapes and jet multiplicities can be expected to show an asymmetry that is preferentially oriented along the beam direction in the $\eta \times \phi$ plane. (At mid-rapidity, the jet sample must be symmetric with respect to the $\eta \rightarrow -\eta$ mirror symmetry, but, in general, it will not be rotationally symmetric in the $\eta \times \phi$ plane.) In the case of a significant transverse collective flow (Fig. 2b), the analogous argument implies the occurrence of jet asymmetries preferentially oriented along the ϕ direction. In principle, the initial-state radiation associated with a hard process can also be shifted in phase space because of a flow field; see Ref. [51] for related work. This work, however, focuses entirely on the final-state radiation underlying jet fragmentation. In general, the size and the orientation of the jet asymmetry depend on how hard processes are spatially distributed in the dynamical expansion case.

Second, flow effects manifest themselves not only in the azimuthal asymmetries of jet observables, but also in inclusive
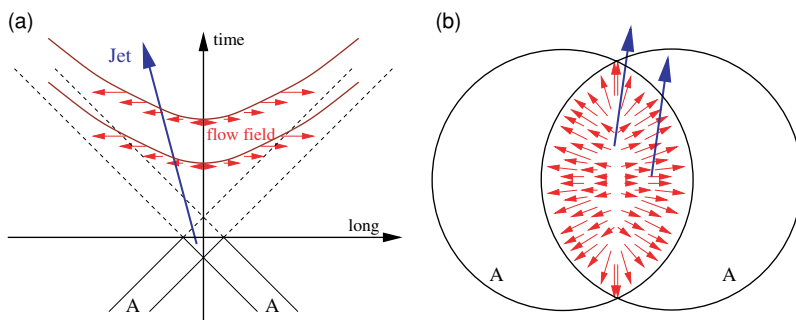

FIG. 2. (Color online) Schematic view of two cases in which jets interact with collective flow fields: (a) If the hard parton is not produced in the Lorentz frame longitudinally comoving with the medium, or if the longitudinal collective flow does not show Bjorken scaling, then the parton interacts with a flow component parallel to the beam. (b) On their propagation in the transverse direction, hard partons generically test transverse flow components, except for the special trajectories that are parallel to the flow field.

high-p_T hadron spectra. In the presence of a flow field, a smaller local energy density is sufficient for the same net momentum transfer to the hard parton and thus for the same medium-induced parton energy loss. This is relevant for the interpretation of the nuclear modification factor in terms of a local energy density. Moreover, hard partons propagating parallel to a flow field can be expected to suffer less momentum transfer and hence less parton energy loss than those traveling along nonparallel trajectories. In this way, low-p_T collective flow can induce high-p_T azimuthal asymmetry by selective elimination of those hard partons that propagate with significant inclination against the flow field. We show that this can yield a sizable additional contribution to high-p_T v_2.

This paper is organized as follows: In Sec. II, we introduce the formalism in which the effects of anisotropic momentum transfer on parton energy loss are calculated. In Sec. III, we calculate the induced asymmetry of the medium-dependent gluon-energy distribution, and in Sec. IV we analyze the resulting anisotropic jet-energy distribution. Up to this point, the medium will be characterized schematically by the momentum scale μ that determines the random momentum transfer to the hard parton and the vector $\mathbf{q}_0$ that specifies the oriented momentum transfer. The ratio q_0/μ indicates the relative strength of collective flow. In Sec. V, we then discuss how to embed this calculation in a dynamical expansion scenario, and we estimate the flow-induced parton energy loss contribution to high-p_T v_2. Finally, we summarize the main conclusions.

II. THE FORMALISM

The starting point of our calculation is the energy distribution of partons into which the initially produced parent parton fragments:

$$\omega \frac{dI^{\text{tot}}}{d\omega\, d\mathbf{k}} = \frac{E_T - \Delta E_T}{E_T} \omega \frac{dI^{\text{vac}}}{d\omega\, d\mathbf{k}} + \omega \frac{dI^{\text{med}}}{d\omega\, d\mathbf{k}}. \quad (2.1)$$

Here, E_T denotes the total energy of the hard parton and $\Delta E_T = \int d\omega\, d\mathbf{k}\, \omega dI^{\text{med}}/d\omega\, d\mathbf{k}$ is that part of the total energy that is redistributed by medium-induced radiation. The radiation spectrum in the vacuum is normalized to $E_T = \int d\omega\, d\mathbf{k}\, \omega dI^{\text{vac}}/d\omega\, d\mathbf{k}$, since, in the absence of a medium, the entire energy E_T of the initial parton resides in the vacuum component. In the presence of a medium, this vacuum contribution is reduced by the factor $(E_T - \Delta E_T)/E_T$. With this prefactor, one finds $\int d\omega\, d\mathbf{k}\omega\ dI^{\text{tot}}/d\omega\, d\mathbf{k} = E_T$, i.e., the total energy radiated always equals the initial energy of the parent parton, irrespective of the strength of medium effects. In this sense, the factor $(E_T - \Delta E_T)/E_T$ ensures energy-momentum conservation.

In the absence of a nuclear environment, the parton fragments according to the distribution $I^{\text{tot}} = I^{\text{vac}}$. In the medium, the parent parton radiates additional gluons because of medium-induced multiple scattering. This medium-induced gluon radiation has been calculated to leading order in $1/E$, resumming an arbitrary number of scattering centers [2–5]. It depends to leading order in $1/E$ on the in-medium path length L and on the average squared transverse momentum transferred to the hard parton per unit path length. The latter

property of the medium is parametrized differently in different approaches, e.g., in terms of the BDMPS transport coefficient $\hat{q}$ [2–4], or as the product of the longitudinal density of scattering centers n_0 along the parton trajectory and their typical momentum transfer μ^2 [4,5]. These parametrizations are known to lead to equivalent results for the medium-induced gluon radiation [9]. In what follows, we use the single-hard scattering approximation, in which the effects of multiple scattering are characterized by the number of effective scattering centers $n_0 L$ times the radiation off a single scattering center. The elastic-scattering cross section is modeled in terms of Debye-screened Yukawa potentials:

$$|a(\mathbf{q})|^2 = \frac{\mu^2}{\pi(\mu^2 + \mathbf{q}^2)^2}. \quad (2.2)$$

The medium-induced gluon radiation is given by Refs. [4,5,9]

$$\omega \frac{dI^{\text{med}}}{d\omega\, d\mathbf{k}} = \frac{\alpha_s}{(2\pi)^2} \frac{4C_R n_0}{\omega} \int d\mathbf{q} |a(\mathbf{q})|^2 \frac{\mathbf{k} \cdot \mathbf{q}}{\mathbf{k}^2}$$

$$\times \frac{-L\frac{(\mathbf{k}+\mathbf{q})^2}{2\omega} + \sin\left[L\frac{(\mathbf{k}+\mathbf{q})^2}{2\omega}\right]}{[(\mathbf{k}+\mathbf{q})^2/2\omega]^2}. \quad (2.3)$$

This radiation spectrum is for a time-independent homogeneous medium. However, it also applies to a time-dependent density of scattering centers if the density n_0 is replaced with an appropriate time average (see Refs. [9,52] and Sec. V A). Moreover, by going step by step through the derivation of Eq. (2.3) given in Ref. [4], we have checked explicitly that Eq. (2.3) holds also for azimuthally anisotropic-scattering potentials in which $|a(\mathbf{q})|^2$ is not a function of $|\mathbf{q}|$ only.

If a flow component is directed orthogonally to the parton trajectory, then the momentum transfer from the medium is anisotropic. We denote by $\vec{q}_0 = (\mathbf{q}_0, q_0^l)$ the directed momentum transfer to the hard parton that is parallel to the spatial components of the flow field $u_\mu(x)$. Here and in the following discussion, transverse vectors lie in the plane orthogonal to the trajectory of the hard parton while longitudinal components are parallel to this trajectory. In the high-energy limit, momentum transfers parallel to the hard parton are negligible. Thus the effect of collective flow on the medium-induced radiation [Eq. (2.3)] can be accounted for by use of an anisotropic scattering potential

$$|a(\mathbf{q})|^2 = \frac{\mu^2}{\pi[(\mathbf{q} - \mathbf{q}_0)^2 + \mu^2]^2}. \quad (2.4)$$

The parameters μ and $|\mathbf{q}_0|$ characterize the strength of the random and directed momentum transfers from the medium to the hard test particle, respectively. The component q_0^l is parallel to the parton trajectory and does not enter our calculation. We work in radial coordinates,

$$d\mathbf{q} = q dq d\varphi, \quad d\mathbf{k} = k dk d\alpha, \quad (2.5)$$

where α denotes the angle between the transverse momenta $\mathbf{k}$ and $\mathbf{q}_0$. The φ integration in Eq. (2.3) can then be done analytically. We always work in the frame longitudinally comoving with the hard parton in which the parton propagates orthogonal to the beam direction.

We now consider more explicitly the case of a longitudinal flow component parallel to the beam direction; see Fig. 3. To
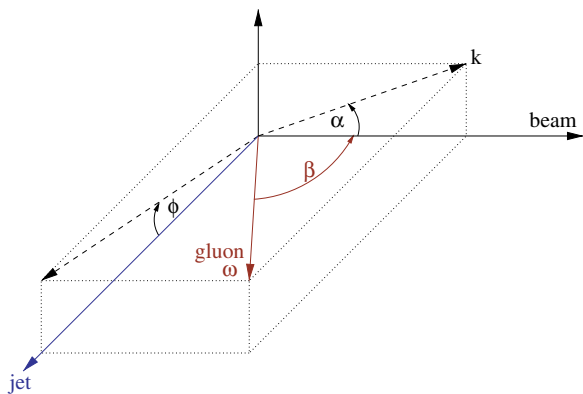
FIG. 3. (Color online) Definition of kinematic variables of a gluon emitted inside a jet cone. Variables are defined in the Lorentz frame that is longitudinally comoving with the jet.

express the radiation spectrum as a function of pseudorapidity η and azimuthal angle ϕ with respect to the center of the jet at $\eta = \phi = 0$, we write the pseudorapidity of an emitted gluon as $\eta = -\ln \tan \beta/2$, where β is the angle between the gluon momentum and the beam axis. We have

$$\tan \beta = \frac{\omega}{k \cos \alpha} \sqrt{1 - \left(\frac{k}{\omega}\right)^2 \cos^2 \alpha}, \quad \tan \phi = \frac{k \sin \alpha}{\sqrt{\omega^2 - k^2}}.$$
(2.6)

Inversion leads to

$$\cos \alpha = \frac{\sinh \eta}{\sqrt{\cosh^2 \eta - \cos^2 \phi}}, \quad \frac{k}{\omega} = \frac{\sqrt{\cosh^2 \eta - \cos^2 \phi}}{\cosh \eta}.$$
(2.7)

The Jacobian for the transformation to jet observables η, ϕ reads

$$k \, dk \, d\alpha = \omega^2 \frac{\cos \phi}{\cosh^3 \eta} d\eta d\phi.$$
(2.8)

Our final expression is

$$\omega \frac{dI^{\mathrm{med}}}{d\omega \, d\eta \, d\phi} = \omega^3 \frac{\cos \phi}{\cosh^3 \eta} \frac{\alpha_s C_R}{\pi^2} \frac{4n_0 \, \mu^2}{\mathbf{k}^2} \int_0^\infty d\mathbf{q}^2 \frac{\frac{L\mathbf{q}^2}{2\omega} - \sin \frac{L\mathbf{q}^2}{2\omega}}{\mathbf{q}^4}$$
$$\times \frac{\mathbf{k}^2[q^2 + \mu^2 + (\mathbf{q}_0 + \mathbf{k})^2] - 2\mathbf{q}^2 \mathbf{k} \cdot (\mathbf{q}_0 + \mathbf{k})}{\left\{[\mathbf{q}^2 + \mu^2 - (\mathbf{q}_0 + \mathbf{k})^2]^2 + 4\mu^2 (\mathbf{q}_0 + \mathbf{k})^2\right\}^{3/2}},$$
(2.9)

where $\mathbf{k}$ and the angle α are given by Eq. (2.7) in terms of η and ϕ. The case of a transverse flow component is obtained by obvious rotations and redefinitions of the vectors in Fig. 3.

III. TRANSVERSE MOMENTUM DEPENDENCE OF THE MEDIUM-INDUCED GLUON RADIATION IN THE PRESENCE OF FLOW

In this section, we discuss the generic properties of the medium-induced gluon radiation [Eq. (2.3)] in the presence of collective flow. To this end, it is convenient to change to dimensionless variables

$$\bar{\kappa} = |\mathbf{k}|/\mu, \quad \bar{q} = |\mathbf{q}|/\mu, \quad \bar{\gamma} = \bar{\omega}_c/\omega, \quad \bar{\omega}_c = \tfrac{1}{2} \mu^2 L.$$
(3.1)

We transform Eq. (2.3) to radial coordinates $d\mathbf{q} = \mu^2 \bar{q} d\bar{q} d\varphi$ and $d\mathbf{k} = \mu^2 \bar{\kappa} \, d\bar{\kappa} d\alpha$, where α denotes the angle between the transverse momenta $\mathbf{k}$ and $\mathbf{q}_0$. Doing the φ integration in Eq. (2.3), we find

$$\omega \frac{dI^{\mathrm{med}}}{d\omega \bar{\kappa} d\bar{\kappa} d\alpha} = \frac{\alpha_s C_R}{\pi^2} 2n_0 L \int d\bar{q}^2 \frac{\bar{q}^2 - \frac{1}{\bar{\gamma}} \sin \bar{\gamma} \bar{q}^2}{\bar{\kappa}^2 \bar{q}^4} \frac{\bar{\kappa}^2 \left[\bar{q}^2 + 1 + \left(\bar{q}_0^2 + \bar{\kappa}^2 + 2\bar{q}_0 \bar{\kappa} \cos \alpha\right)\right] - 2\bar{q}^2 (\bar{\kappa}^2 + \bar{\kappa} \bar{q}_0 \cos \alpha)}{\left\{\left[\bar{q}^2 + 1 - \left(\bar{q}_0^2 + \bar{\kappa}^2 + 2\bar{q}_0 \bar{\kappa} \cos \alpha\right)\right]^2 + 4\left(\bar{q}_0^2 + \bar{\kappa}^2 + 2\bar{q}_0 \bar{\kappa} \cos \alpha\right)\right\}^{3/2}}.$$
(3.2)

In Fig. 4, we plot the medium-induced energy distribution as a function of $\bar{\kappa}^2$ and α for fixed ratios of $\bar{\gamma} = \bar{\omega}_c/\omega$. Here, $\alpha = 0$ denotes the direction of the collective flow vector $\mathbf{q}_0$. Figure 4 shows clearly that more energy is deposited in the direction of the collective flow vector $\mathbf{q}_0$. For the same reason, the energy distribution is depleted in the direction opposite to $\mathbf{q}_0$, i.e., for $\alpha \sim \pi$. For the medium-induced component plotted in Fig. 4, this shows up as a negative contribution, while the total energy distribution (2.1) stays, of course, positive.

For nonzero values of the flow vector $\mathbf{q}_0$, the triple differential gluon distribution (3.2) has a singular behavior for $\bar{\kappa} \to 0$:

$$\lim_{\bar{\kappa} \to 0} \omega \frac{dI^{\mathrm{med}}}{d\omega \, \bar{\kappa} d\bar{\kappa} \, d\alpha} = \begin{cases} +\infty & \text{for} \quad -\frac{\pi}{2} < \alpha < \frac{\pi}{2} \\ -\infty & \text{for} \quad \frac{\pi}{2} < \alpha < \frac{3\pi}{2} \end{cases}.$$
(3.3)

Figure 4 displays only finite values of $\bar{\kappa}$, but the limit (3.3) is consistent with the small-$\bar{\kappa}$ behavior seen in Fig. 4. This singularity is unphysical. It stems from the fact that the formalism leading to Eq. (2.3) calculates medium modifications to a perturbative parton splitting $\propto 1/\mathbf{k}^2$ without regularization of this collinear divergence. At $\bar{\kappa} = 0$, the anisotropic flow field shifts part of this singularity as a positive contribution to the half plane $-\pi/2 < \alpha < \pi/2$ while depleting the region $\pi/2 < \alpha < 3\pi/2$. In the $\eta \times \phi$ plane, Eq. (2.9) integrated over energy shows the same singular structure, namely a positive divergence for $\eta \to 0^+$ and a negative divergence for $\eta \to 0^-$. These two divergences cancel each other if integrated over an arbitrary small neighborhood around $\bar{\kappa} = 0$ (i.e., around $\eta = \phi = 0$). They
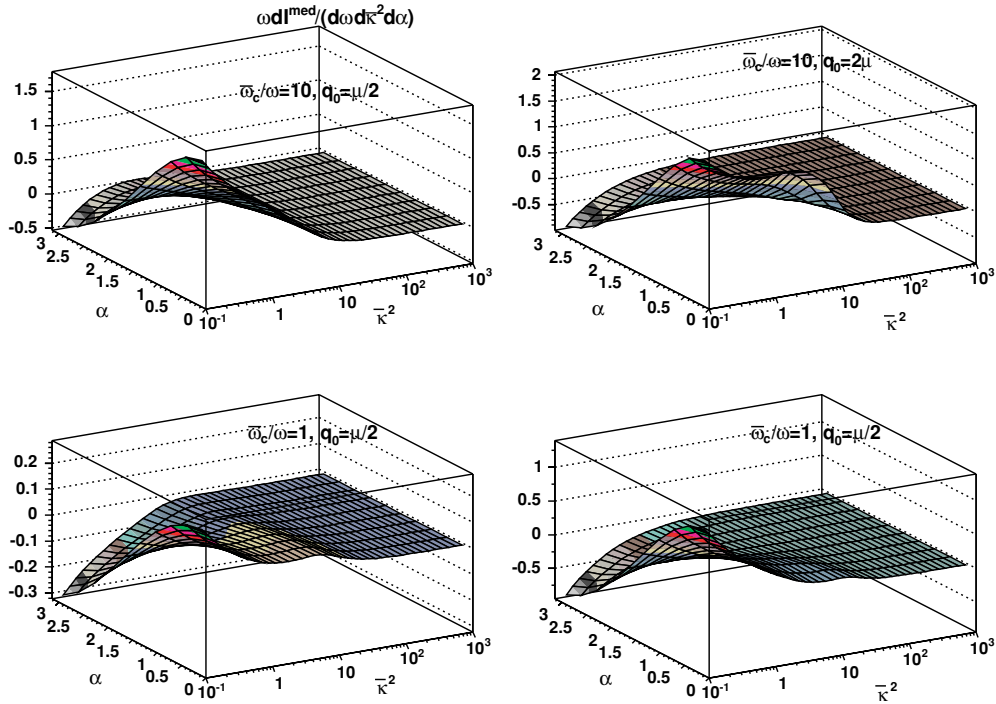
FIG. 4. (Color online) Plot of the medium-induced gluon energy distribution (3.2) as a function of the angle α and rescaled transverse momentum $\bar{\kappa}^2 = \mathbf{k}^2/\mu^2$ for different values of the rescaled gluon energy $\frac{1}{2}\mu^2 L/\omega$ and the collective flow strength q_0. Plots are for $\mu = 2$ GeV and $L = 6$ fm.

represent a very small contribution to the total jet energy (see the discussion below).

In Fig. 5, we plot the gluon-energy distribution (3.2) for a sample of medium-modified jet shapes for which the

orientation $\pm\mathbf{q}_0$ of the collective flow is known but the directions $\mathbf{q}_0$ and $-\mathbf{q}_0$ are equally likely. The figure clearly indicates that the singular behavior for $\bar{\kappa} \to 0$ disappears. For fixed values of $\bar{\gamma} = \bar{\omega}_c/\omega$, the energy distribution has a
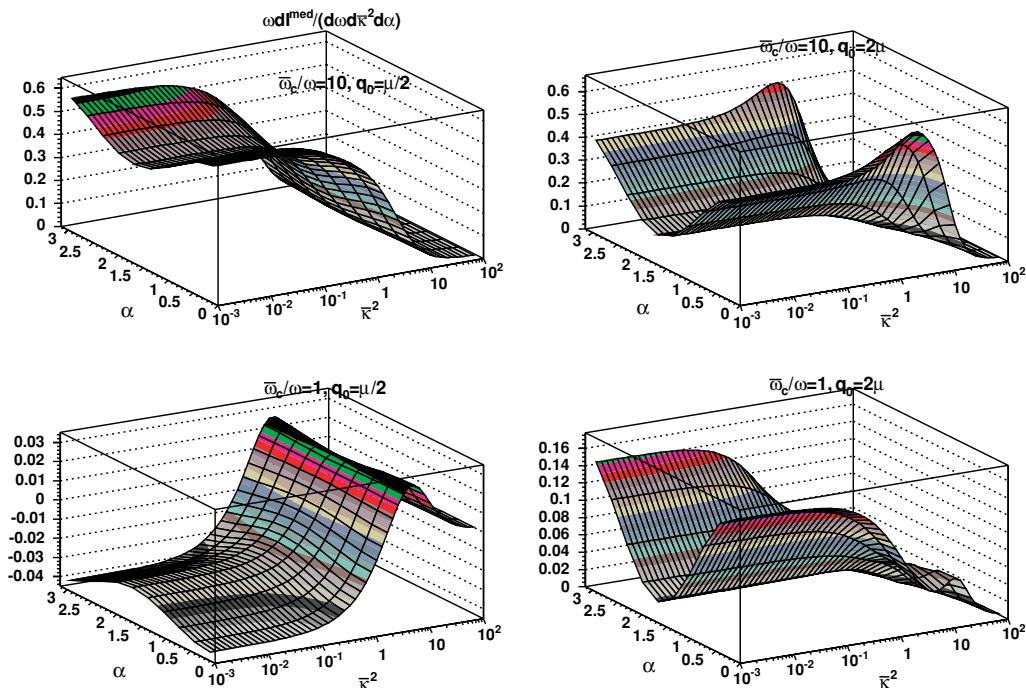

FIG. 5. (Color online) The gluon-energy distribution (3.2) for the same parameters as in Fig. 4, but averaged over the cases $\mathbf{q}_0$ and $-\mathbf{q}_0$.

finite constant value for $\bar{\kappa} \to 0$. By construction, the obtained distribution is symmetric around $\alpha = \pi/2$, but it shows a marked angular dependence.

IV. COLLECTIVE FLOW LEADS TO ANISOTROPIC JET-ENERGY DISTRIBUTIONS

In this section, we discuss the medium modification of jet-energy distributions. Our starting point is the gluon-energy distribution (2.1). We constrain the vacuum contribution $I^{\rm vac}$ of this spectrum by data on the energy fraction of a jet contained in a subcone of radius $R = \sqrt{\eta^2 + \phi^2}$:

$$\rho_{\rm vac}(R) \equiv \frac{1}{N_{\rm jets}} \sum_{\rm jets} \frac{E_T(R)}{E_T(R=1)}$$

$$= 1 - \frac{1}{E_T} \int d\omega \int^\omega d\mathbf{k} \, \Theta\left(\frac{k}{\omega} - R\right) \omega \frac{dI^{\rm vac}}{d\omega \, d\mathbf{k}}. \tag{4.1}$$

For the jet shape $\rho_{\rm vac}(R)$, we use the parametrization [53] of the Fermilab $D0$ Collaboration determined for jets in the range $\approx 50 < E_t < 170$ GeV and opening cones $0.1 < R < 1.0$:

$$\rho_{\rm vac}^{(D0)}(R) = AR^{0.1} + BR^{0.3} + CR^{0.5} + DR^{0.7} + ER^{0.9}, \tag{4.2}$$

where

$$A(E_T) = -3.47 + 0.85 \times 10^{-2} E_T - 0.25 \times 10^{-4} E_T^2,$$
$$D(E_T) = 3.30 - 0.77 \times 10^{-2} E_T + 0.22 \times 10^{-4} E_T^2, \quad \tag{4.3}$$
$$B = 9.75, \quad C = -8.32, \quad E = -0.30.$$

At very small values of R, this parametrization turns negative. We cure this unphysical behavior by matching Eq. (4.2) with a third-order polynomial that smoothly interpolates to $\rho_{\rm vac}(R = 0) = 0$:

$$\rho_{\rm vac}(R) = \begin{cases} \rho_{\rm vac}^{(D0)}(R) & \text{for} \quad R > 0.04 \\ aR^2 + bR^3 & \text{for} \quad R < 0.04. \end{cases} \tag{4.4}$$

We fix the parameters a and b in Eq. (4.4) by requiring that $\rho_{\rm vac}(R)$ and its first derivative are continuous.

The medium-induced part of the jet-energy distribution is determined from Eq. (2.9):

$$\frac{dE^{\rm med}}{d\eta \, d\phi} = \int_0^E d\omega \, \omega \frac{dI^{\rm med}}{d\omega \, d\eta \, d\phi}. \tag{4.5}$$

It contains a fraction $\Delta E_T/E_T$ of the available jet energy:

$$\Delta E_T = \int d\eta \int d\phi \frac{dE^{\rm med}}{d\eta \, d\phi}. \tag{4.6}$$

For the vacuum contribution, the corresponding distribution is defined by the vacuum jet shape [Eq. (4.4)]:

$$\frac{dE^{\rm vac}}{d\eta \, d\phi} = (E_T - \Delta E_T) \frac{d\rho_{\rm vac}}{2\pi R \, dR}. \tag{4.7}$$

Here, the prefactor $(E_T - \Delta E_T)$ ensures energy conservation.

A. Harmonic expansion of jet-energy distribution

In this subsection, we characterize the flow-induced asymmetry of jet-energy distributions in terms of a harmonic analysis in the $\eta \times \phi$ plane. We introduce radial coordinates in this plane:

$$R = \sqrt{\eta^2 + \phi^2}, \tag{4.8}$$

$$\alpha' = \arctan(\phi/\eta). \tag{4.9}$$

The flow field points in the direction $\alpha' = 0$. We calculate now the jet-energy distribution in the $\eta \times \phi$ plane:

$$\frac{dE_T}{R \, dR \, d\alpha'} = \frac{dE_T}{d\eta \, d\phi} = \frac{dE_T^{\rm vac}}{d\eta \, d\phi} + \frac{dE_T^{\rm med}}{d\eta \, d\phi}. \tag{4.10}$$

In the absence of flow, the radiation spectrum (3.2) is rotationally symmetric in the coordinates $\bar{\kappa}$ (or $\mathbf{k}$) and α. However, the energy distribution (4.10) is elongated in the ϕ direction because of the Jacobian (2.8) in the coordinate transform. In general, this reduces the effect of η broadening that is due to longitudinal flow, and it can be corrected for analytically. However, this asymmetry is rather small ($<10\%$) for small cone sizes ($R < 0.3$), and can be neglected safely in the following discussion. To analyze the asymmetries of jet-energy distribution (4.10) in the $\eta \times \phi$ plane, we use a harmonic expansion:

$$\frac{dE_T}{R \, dR \, d\alpha'} = E^{(0)}(R) + 2 \sum_{n=1}^\infty E^{(n)}(R) \cos(n\alpha'). \tag{4.11}$$

The coefficients proportional to $\sin(n\alpha')$ cancel since the jet-energy distribution (4.10) is by construction symmetric with respect to $\alpha' \to -\alpha'$.

For illustration, we now study the case of a jet of total energy $E_T = 100$ GeV traversing a medium in which $\Delta E_T = 23$ GeV were redistributed in phase space because of medium effects. This parton energy loss is obtained, e.g., for an in-medium path length of nuclear size ($L = 6$ fm), a momentum transfer per scattering center of $\mu = 1$ GeV, and a collective flow effect of the same size $q_0 = \mu$, with an effective coupling constant in Eq. (2.3) fixed to $n_0 L \alpha_s C_R = 1$. This corresponds to a gluon jet ($C_R = C_A = 3$) with a reasonable perturbative coupling $\alpha_s = 1/3$ and an opacity $n_0 L = 1$. Changes in the coupling can be absorbed in a redefinition of the density of scattering centers. Recent model comparisons with RHIC data support the picture of an opaque medium that may result in significantly larger medium-induced modifications than the ones modeled here. However, to illustrate the sensitivity of jet-shape measurements, we prefer to work with a sizable but relatively small effect.

In Fig. 6, we show the first six harmonic coefficients extracted for the jet-energy distribution (4.11). Since the vacuum term [Eq. (4.4)] is rotationally symmetric, it contributes only to $E^{(0)}(R)$. The total jet energy is obtained by integration of this zeroth moment over R. The shape of the medium-induced part of $E^{(0)}(R)$ is negative at small R, which indicates the medium-induced depletion of the jet energy in this region of phase space. This is the result of multiple scattering that broadens the jet-energy distribution by moving a fraction of the total jet energy to larger values of R. The higher moments
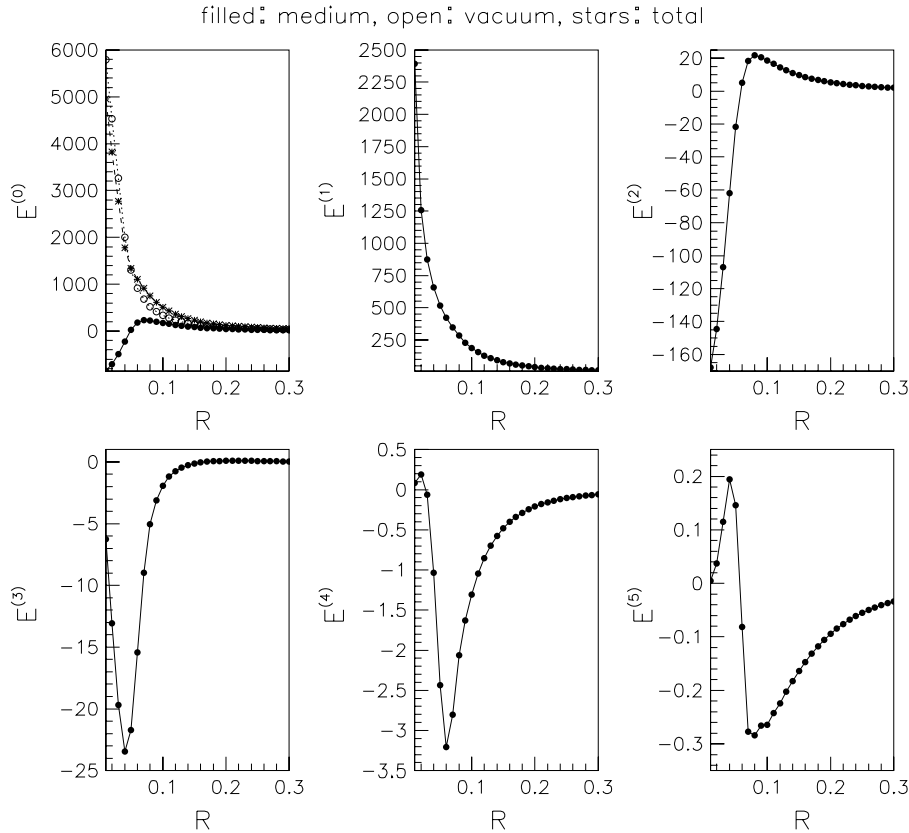
FIG. 6. The harmonic coefficients that characterize the asymmetry of the jet-energy distribution of a 100-GeV jet in the $\eta \times \phi$ plane. Parameters are given in the text.

$E^{(n)}(R)$, $n \geqslant 1$, contain information about asymmetries in the energy distribution but do not contribute to the total jet energy. For the case of averaged jet samples over opposite flow directions $\mathbf{q}_0$ and $-\mathbf{q}_0$, the odd harmonic moments vanish while the even ones stay the same. The absolute size of the harmonic moments decreases by approximately 1 order of magnitude per moment n. This indicates that the first and second moments are sufficient to characterize the asymmetries of the jet shape. We note that to reconstruct the jet shape from the moments $E^{(0)}(R)$, $E^{(1)}(R)$, and $E^{(2)}(R)$, we have to integrate over $R\,dR$—this tames significantly the large values of these moments in the region $R \sim 0$. We expect that most of the experimentally accessible structures lie in the range $0.05 < R < 0.3$.

The technical advantage of the harmonic expansion (4.11) is that the unphysical singularities of the vacuum contribution (4.7) and the medium contribution (4.5) at $R = 0$ can be removed easily. In the harmonic coefficients $E^{(n)}(R)$ of Eq. (4.11), these singularities appear in the odd moments at $R \to 0$. The smallest value calculated for Fig. 6 is for $R = 0.01$. For much smaller values of R, we find numerically $E^{(1)}(R = 10^{-4}) \sim 2 \times 10^5$ and $E^{(1)}(R = 10^{-6}) \sim 2 \times 10^7$. For the figures presented in this work, we cut off this artificial small-R structure in the harmonics and plot the jet-energy distribution according to Eq. (4.11). As explained above, the presence of these singularities indicates that our formalism becomes unreliable in the collinear region of very small R. For the arguments in this paper, this is not a problem since only a small amount ($<5\%$ for $R < 0.01$) of the total jet energy lies inside this small phase-space region.

B. Profile and displacement of jet-energy distribution

In general, collective flow shifts the calorimetric jet center and distorts the shape of the jet-energy distribution. Any calorimetric jet-finding algorithm can be expected to center the cone around the medium-displaced jet center. Figure 7 shows this displacement $\Delta\eta$ as a function of the collective flow
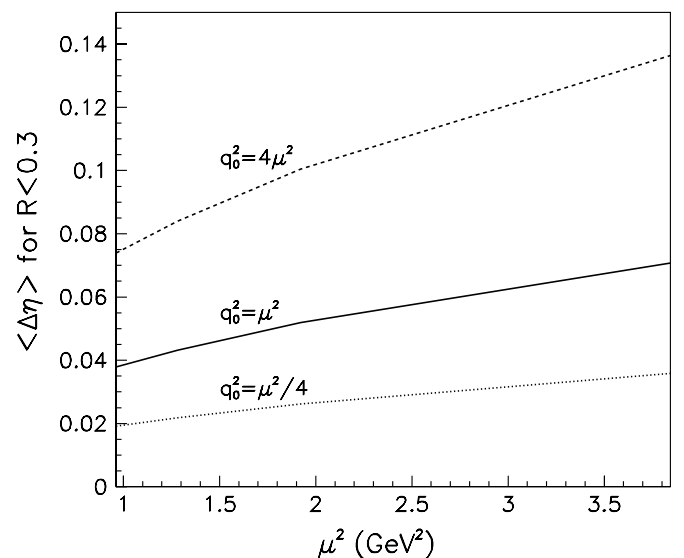

FIG. 7. The displacement $\Delta\eta$ of the calorimetric center of the jet cone as a function of collective flow strength q_0 and average momentum transfer μ from the medium.
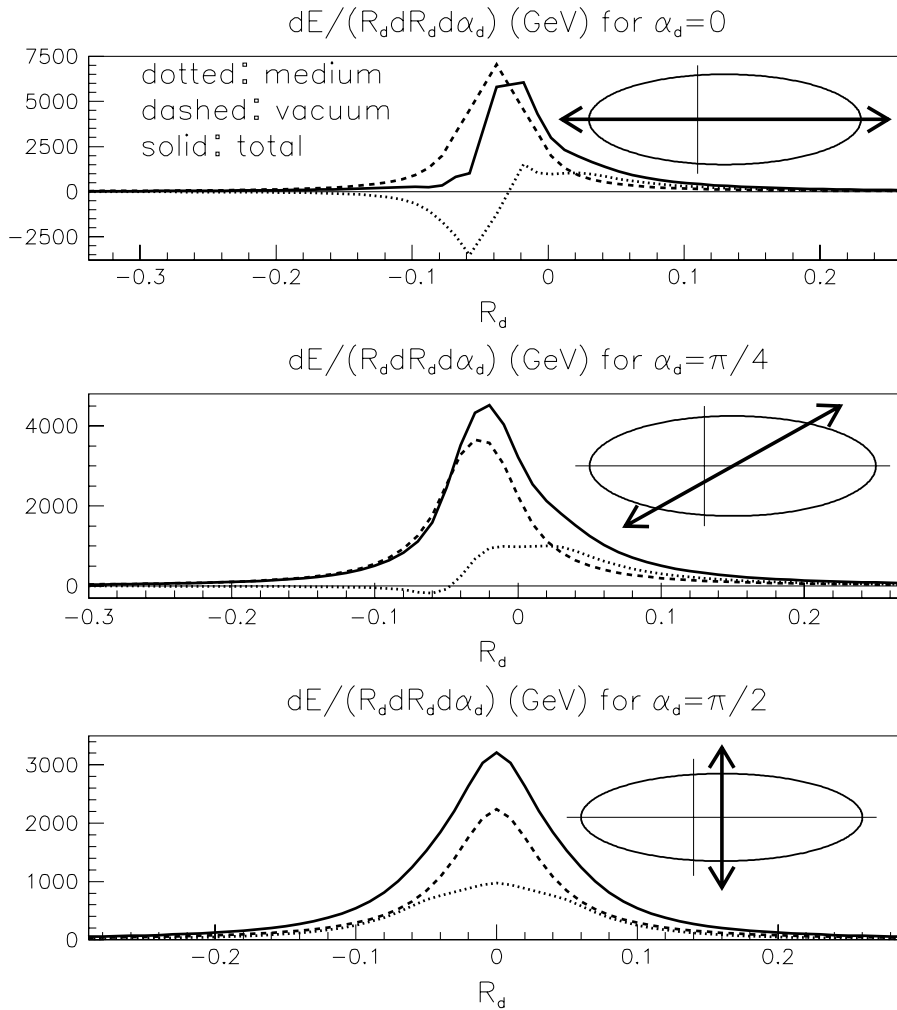
FIG. 8. The jet-energy distribution (4.10), plotted along different cuts in the $\eta \times \phi$ plane, as indicated. The variables R_d and α_d denote the distance and orientation, respectively, with respect to the displaced calorimetric center of the jet cone. Parameters are the same as those of Fig. 6.

strength, calculated by averaging the jet-energy distribution (4.10) over a central cone of size $R < 0.3$. For a fixed average momentum transfer μ per scattering center, the displacement grows approximately linearly with the directed momentum transfer q_0. Also, $\Delta \eta$ grows approximately linear with the average momentum transfer μ for a fixed ratio q_0/μ. The overall size of the displacement is rather small: A displacement of size $\Delta \eta = 0.1$ results only for rather large parameter values (e.g., $q_0^2 = 4\mu^2 = 8 \text{ GeV}^2$), that correspond to a large medium-induced average energy loss ($\Delta E_T \approx 62 \text{ GeV}$). This is consistent with the picture that the most energetic jet fragments are radiated collinear. These energetic components that dominate the energy distribution are shifted very little in the $\eta \times \phi$ plane even if they pick up a significant transverse momentum.

In Fig. 8, we show different one-dimensional cuts through the jet-energy distribution (4.10). These cuts go through the displaced jet center and are quantified by the radial coordinates R_d and α_d of the displaced center. Along the beam direction ($\alpha_d = 0$), the jet-energy distribution is shifted with the flow field; see Fig. 8. The medium-induced part of the jet-energy distribution takes negative values in the region of phase space that is depleted because of medium effects. We observe in particular a pronounced long tail of the distribution in the direction of the flow. We attribute this tail

to the soft jet fragments that can be displaced significantly in η by a typical momentum transfer from the medium. In contrast, in the direction orthogonal to the collective flow, one observes a numerically small medium-induced broadening of the jet-energy distribution, which is not accompanied by a displacement.

For measurements at mid-rapidity, one can obtain experimentally only the orientation but not the direction of the collective flow component. Then each jet of the sample is positioned around its calorimetric center that is shifted with equal probability in the positive or negative beam direction. We have given numerical results for this case already in a previous exploratory study [46]. The main conclusion is that the jet-energy distribution can broaden significantly along the orientation of the flow. The analogous conclusion holds for the case of a strong transverse collective flow field, in which only $\phi \rightarrow -\phi$-symmetrized samples are measurable.

C. Asymmetries in the jet-multiplicity distributions

If the jet-energy distribution is sensitive to collective flow, then high-p_T particle correlations and jet multiplicities should be sensitive too. From the medium-induced gluon-energy distribution (2.7), we can explore this sensitivity qualitatively
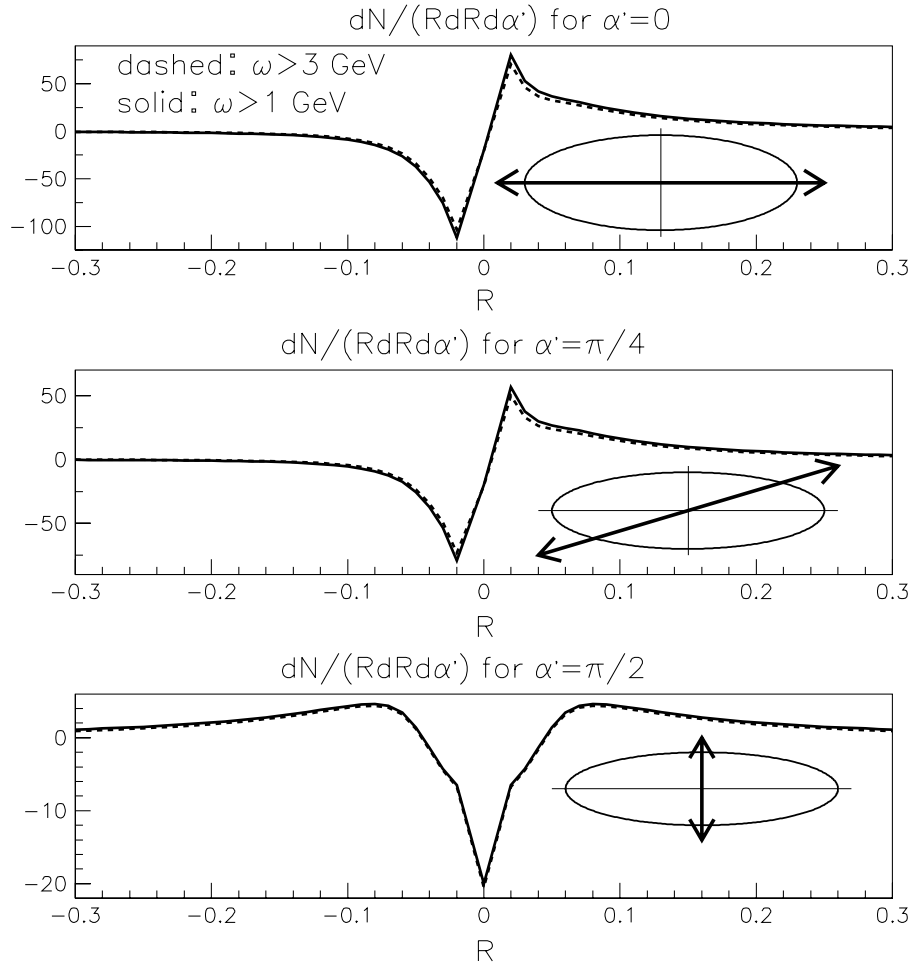
FIG. 9. The medium-induced contribution (4.12) to the total jet-multiplicity distribution for different cuts in the $\eta \times \phi$ plane. Parameters are the same as those of Fig. 6.

by calculating the number of medium-induced gluons emitted with a gluon energy $\omega > \omega_{\mathrm{cut}}$. In the $\eta \times \phi$ plane, this medium-induced multiplicity distribution reads

$$N(\phi, \eta, \omega_{\mathrm{cut}}) \equiv \frac{dN(\omega_{\mathrm{cut}})}{d\eta\,d\phi} = \int_{\omega_{\mathrm{cut}}}^{E} d\omega\, \frac{dI^{\mathrm{med}}}{d\eta\,d\phi}. \qquad (4.12)$$

Relating Eq. (4.12) to an experimentally accessible quantity requires a hadronization model and faces uncertainties that have been mentioned before [9]. In Fig. 9, we plot the medium-induced modification (4.12) of the jet multiplicity for the case of a collective flow in the positive beam direction. The qualitatively expected effects are illustrated clearly. In the beam direction, there is a marked reshuffling from negative to positive rapidities that is due to collective flow effects. In the direction orthogonal to the beam, there is a somewhat smaller reshuffling from smaller to larger cone sizes: This is the result of multiple scattering in an isotropic medium, which leads to a characteristic broadening of the jet-multiplicity distributions.

As a result of the eikonal approximation that underlies the calculation of the medium-induced gluon-energy distribution (2.7), the leading hard parton does not change its direction because of medium effects. This corresponds to the assumption that the leading hadron of the jet is located at $\eta \approx \phi \approx 0$. Then, Fig. 9 provides an estimate of the rotational asymmetry of hadron production associated with a high-p_T trigger particle. Recently, two-particle correlations and their possible medium

modifications were discussed in several approaches [54–58]. From the present study, we expect flow-induced asymmetries to affect such two-particle correlation measurements in nucleus-nucleus collisions. In particular, asymmetries are expected in multiplicity distributions associated with high-p_T trigger particles and in leading two-particle correlations [46].

V. PARTON ENERGY LOSS IN DYNAMICAL SIMULATIONS

A. A proposal to determine parton energy loss from the energy-momentum tensor

In a realistic dynamical case of a nucleus-nucleus collision, the produced hard parton propagates through a medium of varying spatial and temporal energy density $\epsilon(\mathbf{r}, z, \xi)$ and varying collective flow $u_\mu(\mathbf{r}, z, \xi)$. Thus its parton energy loss will depend on the spatial position $\vec{r}_0$ of its production point (the production time is $\xi \sim 0$ for hard processes) and the orientation $\vec{n}$ of its trajectory:

$$\vec{r}(\xi) = \vec{r}_0 + \xi\vec{n}. \qquad (5.1)$$

In the absence of collective flow, numerical studies of the medium-induced gluon-energy distribution have shown that the medium-induced gluon radiation for a medium of time-dependent density is equivalent to that of a static medium

whose density has been rescaled appropriately. This rescaling requires the determination of the linearly line-averaged characteristic gluon energy along the trajectory $\vec{r}(\xi)$ [28,52,59]:

$$\omega_c\left[\vec{r}(\xi)\right] = \int_0^\infty d\xi \, \xi \, c \, \epsilon^{3/4}[\vec{r}(\xi), \xi]. \qquad (5.2)$$

Here, we have expressed the BDMPS transport coefficient (1.1) in terms of the local energy density, $\hat{q}(\vec{r}, \xi) = c \, \epsilon^{3/4}(\vec{r}, \xi)$. In the same way, we can determine the time-averaged total transverse momentum squared

$$(\hat{q}L)\left[\vec{r}(\xi)\right] = \int_0^\infty d\xi \, c \, \epsilon^{3/4}[\vec{r}(\xi), \xi], \qquad (5.3)$$

and construct the quotient $\omega_c L = 2\omega_c^2/\hat{q}L$. The probability distribution that an additional fraction ΔE of the parton energy is lost because of medium-induced scattering depends on ω_c and $\omega_c L$. A numerical routine for its calculation is publicly available [9]. The characteristic gluon energy of Eq. (5.2) and momentum broadening of Eq. (5.3) can be related to the model parameters entering the medium-induced gluon-energy distribution (2.3) by means of

$$\omega_c = \tfrac{1}{2}\hat{q}L^2 = \tfrac{1}{2}(n_0 L)\,\mu^2 L, \qquad (5.4)$$

$$\hat{q}L = (n_0 L)\mu^2. \qquad (5.5)$$

Remarkably, the time averages (5.2) and (5.3) do not require a priori knowledge of the in-medium path length L. In the case of a time-independent energy density of a medium of finite size, $\epsilon(\mathbf{r}) \propto \Theta(|\mathbf{r}| - L)$, one recovers the expressions for the static case. For further details of how to relate parton energy loss in a time-dependent medium to an equivalent time-independent calculation, we refer the reader to Refs. [9,52,60].

Collective flow is an additional source of momentum transfer to the hard parton and will result in additional parton energy loss. To account for this effect, we suggest to replace the energy density in Eq. (5.2) with the relevant boosted component of the energy-momentum tensor (1.2). To be more specific, we consider the component $T^{n_\perp n_\perp}$, where $n_\perp$ is orthogonal to the trajectory (5.1) of the hard parton:

$$T^{n_\perp n_\perp} = p(\epsilon) + [\epsilon + p(\epsilon)]\,\frac{\vec{\beta}_\perp^2}{1 - \beta^2}. \qquad (5.6)$$

Here, $\beta_\perp$ is the spatial component of the collective flow field that is orthogonal to the parton trajectory. In general, all quantities entering Eq. (5.6) will depend on space and time. In the absence of flow effects, $\beta_\perp = 0$, the component $T^{n_\perp n_\perp} = p$ determines the pressure and hence it determines by means of the equation of state the energy density $\epsilon(p)$ entering Eqs. (5.2) and (5.3). For finite flow $\beta_\perp$, our proposal is to use $\epsilon(T^{n_\perp n_\perp})$ instead of $\epsilon(p)$ in evaluating the characteristic gluon energy and momentum broadening:

$$\hat{q} = c\epsilon^{3/4}(p) \longrightarrow \hat{q} = c\epsilon^{3/4}(T^{n_\perp n_\perp}). \qquad (5.7)$$

This is consistent with what is known from analytical estimates and numerical studies about the dependence of parton energy loss on momentum transfer from the medium. For the determination of jet asymmetries in a dynamical case, relation (5.6), one has to determine the relative strength of the random and directed momentum transfers in Eq. (2.3). For

a feasible model, q_0/μ should increase monotonically with $\{[\epsilon + p(\epsilon)]/p(\epsilon)\}[\vec{\beta}_\perp^2/(1 - \beta^2)]$.

B. Low-p_T elliptic flow induces high-p_T azimuthal asymmetry

In general, a hard parton will suffer less energy loss if it propagates on a trajectory parallel to the flow field. Thus, for the same medium-induced suppression, the azimuthal asymmetry at high transverse momentum becomes larger when the contribution of the collective flow field is increased. To estimate the size of this effect, we consider a simple two-dimensional model. The hard parton is produced at an arbitrary position (x_0, y_0) in the transverse plane according to the nuclear overlap. It propagates in its longitudinally comoving rest frame in the transverse direction $\vec{n} = (\cos\varphi, \sin\varphi)$, along the trajectory

$$\mathbf{r}_0(\xi) = (x_0 + \xi\cos\varphi, y_0 + \xi\sin\varphi). \qquad (5.8)$$

For simplicity, we assume that the longitudinally comoving rest frame of this hard parton is the longitudinal rest frame of the medium. Then there is only a transverse, but not a longitudinal, flow component. For the BDMPS transport coefficient that includes collective flow effects, we make the ansatz

$$\hat{q}(\xi) = q_{nf} + q_f|u_T[\mathbf{r}_0(\xi)] \cdot \mathbf{n}_T|^2. \qquad (5.9)$$

Here q_f and q_{nf} stand for the flow and nonflow components to $\hat{q}$, and the two-dimensional vector $\mathbf{n}_T$ is orthogonal to the trajectory (5.8) and projects out the corresponding transverse component of the collective flow field $u_T[\mathbf{r}_0(\xi)]$. We discuss now the motivation for this ansatz. In the absence of collective flow, q_{nf} defines the time-averaged BDMPS transport coefficient of the dynamically equivalent static scenario, as specified in the discussion of Eqs. (5.2) and (5.3). Thus ansatz (5.9) can account for one of the main effects of longitudinal expansion, namely the time-dependent decrease of scattering centers. In the presence of collective flow, there is an additional momentum transfer orthogonal to the parton trajectory and hence parallel to $\vec{n}_T = (-\sin\varphi, \cos\varphi)$. Since the BDMPS transport coefficient denotes the squared average momentum transfer per unit path length, this contribution enters quadratically, $|u_T[\mathbf{r}_0(\xi)] \cdot \mathbf{n}_T|^2$. For a small collective flow field, this quadratic dependence is consistent with the more general ansatz (5.6).

For an exploratory model study, we use a blast-wave parametrization of the hadronic freeze-out stage of the collision [45]. The transverse density distribution of the produced matter is specified by

$$\Omega(r, \phi_s) = \frac{1}{1 + \exp\left(\frac{\hat{r}-1}{a_s}\right)}, \qquad (5.10)$$

where $\hat{r} = \hat{r}(r, \phi_s)$ denotes a rescaled elliptic position vector:

$$\hat{r}(r, \phi_s) = \sqrt{\frac{x^2}{R_x^2} + \frac{y^2}{R_y^2}}. \qquad (5.11)$$

Here, R_x and R_y are the extensions of the collision region in the reaction plane and orthogonal to it, respectively, ϕ_s is
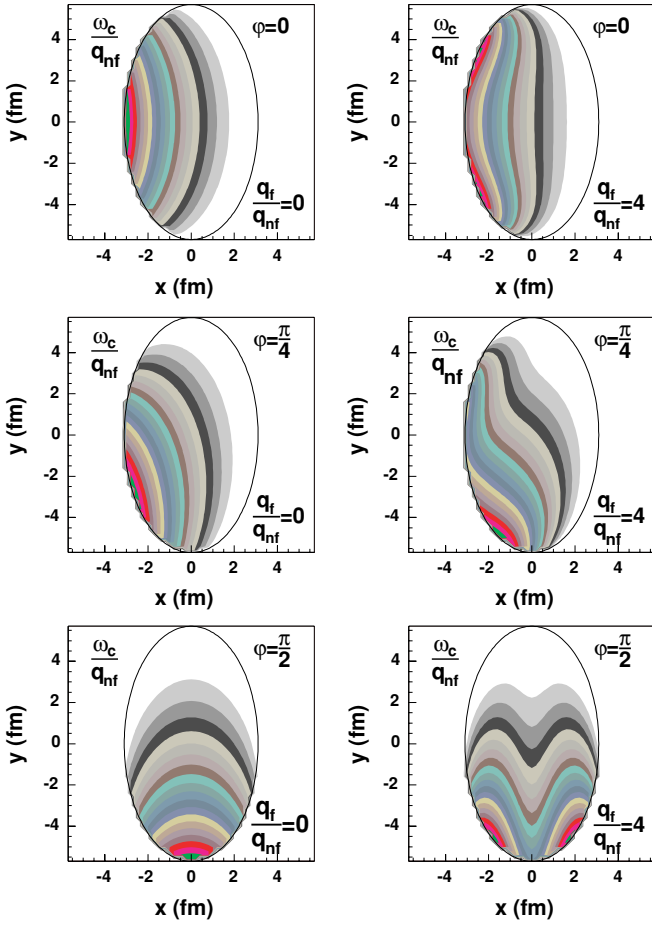
FIG. 10. (Color online) Contour plots of the characteristic gluon energy (5.14) as a function of the production point $\mathbf{r}_0 = (x, y)$ of the hard parton and for different angles $\varphi = 0, \pi/4, \pi/2$ of its trajectory. The dependence of ω_c on the relative flow strength q_f/q_{nf} indicates the extent to which hard partons can escape with less energy loss on trajectories parallel to the flow field. See text for more details.

the azimuthal angle with respect to the reaction plane, and we write transverse positions (x, y) in radial coordinates $x = r \cos \phi_s$ and $y = r \sin \phi_s$. We choose a sharp, almost boxlike, density distribution with $a_s = 0.002$. For the flow field $u_\mu(x)$, we assume a longitudinal Bjorken expansion and we use the standard notation

$$u_\mu(x) = (\cosh \eta \cosh \rho, \sinh \rho \cos \phi_b,$$
$$\sinh \rho \sin \phi_b, \sinh \eta \cosh \rho). \quad (5.12)$$

The coordinate η denotes the longitudinal space-time rapidity, and we work at mid-rapidity $\eta = 0$; ϕ_b defines the orientation that is orthogonal to the elliptic freeze-out surface assumed in the model, $\tan \phi_s = \tan \phi_b (R_y/R_x)^2$. The transverse flow is parametrized as

$$\rho(r, \phi_s) = \hat{r} [\rho_0 + \rho_a \cos(2\phi_b)], \quad (5.13)$$

where $\rho_0 = 0.88$, and $\rho_a = 0.048$ for semiperipheral Au + Au collisions [45]. For the transverse radius parameters, we do not use the extension at freeze-out, but the initial transverse radii for an impact parameter $b = 7$ fm, namely $R_x = 3.1$ fm and $R_y = 5.6$ fm.
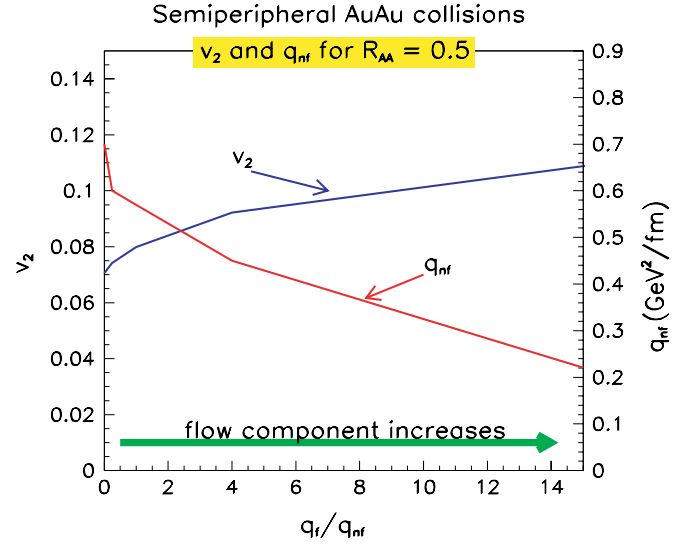

FIG. 11. (Color online) The dependence of elliptic flow v_2 and the nonflow component of the BDMPS transport coefficient q_{nf} on the relative flow strength q_f/q_{nf}, for the case of a nuclear modification factor $R_{AA} = 0.5$ in semiperipheral Au + Au collisions. The calculation is done at fixed transverse momentum $p_T = 7$ GeV.

With this input, we calculate the characteristic gluon energy and average transverse momentum squared for a parton trajectory (5.8) in a medium characterized by its density distribution (5.10) and its collective flow field (5.12). With ansatz (5.9) for the BDMPS transport coefficient, we find

$$\omega_c(\mathbf{r}_0, \varphi) = \int_0^\infty d\xi \, \xi \hat{q}(\xi) \, \Omega[\mathbf{r}(\xi), \xi], \quad (5.14)$$

$$(\hat{q}L)(\mathbf{r}_0, \varphi) = \int_0^\infty d\xi \, \hat{q}(\xi) \, \Omega[\mathbf{r}(\xi), \xi]. \quad (5.15)$$

For a qualitative estimate of the size of parton energy loss, one can use the pocket formula $\Delta E \approx \alpha_s \omega_c$ [29]. This motivates one to investigate $\omega_c(\mathbf{r}_0, \varphi)$ as a function of the production point $\mathbf{r}_0$ of the hard parton for different orientations φ of the parton trajectory. As seen from Eq. (5.9), ω_c depends linearly on q_{nf} and on the relative flow strength q_f/q_{nf}. As this flow strength is increased, ω_c increases for parton trajectories that are not parallel to the flow field. Thus the distortions seen in Fig. 10 provide a first indication of the extent to which parton energy loss depends on a transverse flow field and affects the azimuthal distribution of inclusive hadron spectra.

To estimate the effects of transverse flow, we calculated from Eqs. (5.14) and (5.15) the relative suppression of hadronic spectra that is due to medium-induced parton energy loss:

$$N(x_0, y_0, \varphi, p_T) = \frac{d\sigma^{\text{med}}}{dp_T} \bigg/ \frac{d\sigma^{\text{vac}}}{dp_T}. \quad (5.16)$$

Our evaluation of Eq. (5.16) follows Ref. [9]: We assume a power law $d\sigma^{\text{vac}}/dp_T \propto 1/p_T^7$, and we calculate the medium modification by means of the quenching weights [9,61,62] that depend on Eqs. (5.14) and (5.15). The integral of Eq. (5.16) over $\mathbf{r}_0$ and φ weighted with the density of production points determines the nuclear modification factor R_{AA}. We adjust

the nonflow component q_{nf} such that $R_{AA} = 0.5$ that is the experimentally observed value for semiperipheral collisions of impact parameter $b = 7$ fm. The results shown in Fig. 11 were obtained for $p_T = 7$ GeV and $\alpha_s = 1/3$. They illustrate two qualitative effects of transverse flow: First, low-p_T elliptic flow induces an additional contribution to high-p_T azimuthal asymmetry. This effect may reduce significantly the discrepancy of models of parton energy loss [31,32] in accounting for high-p_T v_2. Second, the presence of collective flow diminishes strongly the local energy density $\epsilon \propto q_{nf}^{4/3}$ of the medium required for a nuclear modification factor R_{AA} of fixed size.

VI. CONCLUSION

In general, hard initially produced partons do not stay in the locally comoving rest frame of the QCD matter generated in a nucleus-nucleus collision. Rather, they propagate through a matter that has collective velocity components orthogonal to the parton trajectory. The resulting flow-induced directed momentum transfer can modify parton splitting significantly. Here we have studied this effect by calculating the triple-differential medium-induced gluon-energy distribution (2.9) radiated off a hard parton as a function of gluon energy, gluon transverse momentum, and azimuthal angle with respect to the flow field. Directed momentum transfers lead to a marked asymmetry of the medium-induced energy distribution, since partonic fragmentation moves significantly with the direction of the collective flow field: See Sec. III.

From the medium-induced gluon radiation spectrum (2.3) and simple assumptions about the dynamical evolution of the matter produced in nucleus-nucleus collisions, we have reached several qualitative conclusions of phenomenological

relevance. In particular, as discussed in Sec. IV, flow-induced distortions of parton fragmentation will be experimentally accessible in calorimetric jet measurements, multiplicity distributions associated with high-p_T trigger particles, and leading two-hadron correlation functions. Moreover, as seen in Fig. 11, different combinations of local energy density and collective flow can account for the same suppression of single inclusive hadron spectra. This illustrates the generic argument of Subsec. V A that the strength of parton energy loss is not governed by the local energy density, but the rather by the local energy-momentum tensor (1.2). Flow effects can also contribute appreciably to the size of the high-p_T v_2 that has been underpredicted in recent model comparisons [31,32].

In general, the effects of medium-induced parton energy loss depend on time-integrated properties of the medium; See Subsec. V A. Thus a more quantitative study of flow-induced parton energy loss effects requires a realistic model of the dynamical evolution of the collision region. It also requires information about the spatial distribution of hard processes in the produced matter. Determining this information is a challenge that—in an interplay of theory and further data analysis at RHIC and the LHC—should come within reach in the near future. We hope that our work is of use for further studies in this direction and in particular for relating the dynamics of a hydrodynamical medium to the dynamics of hard processes in that medium, work that was started in Refs. [63,64].

ACKNOWLEDGMENTS

[1] M. Gyulassy and X. N. Wang, Nucl. Phys. **B420**, 583 (1994).

[2] R. Baier, Y. L. Dokshitzer, A. H. Mueller, S. Peigne, and D. Schiff, Nucl. Phys. **B484**, 265 (1997).

[3] B. G. Zakharov, JETP Lett. **65**, 615 (1997).

[4] U. A. Wiedemann, Nucl. Phys. **B588**, 303 (2000).

[5] M. Gyulassy, P. Levai, and I. Vitev, Nucl. Phys. **B594**, 371 (2001).

[6] X. N. Wang and X. F. Guo, Nucl. Phys. **A696**, 788 (2001).

[7] U. A. Wiedemann, Nucl. Phys. **A690**, 731 (2001).

[8] R. Baier, Y. L. Dokshitzer, A. H. Mueller, and D. Schiff, Phys. Rev. C **64**, 057902 (2001).

[9] C. A. Salgado and U. A. Wiedemann, Phys. Rev. D **68**, 014008 (2003).

[10] C. A. Salgado and U. A. Wiedemann, Phys. Rev. Lett. **93**, 042301 (2004).

[11] K. Adcox *et al.* (PHENIX Collaboration), Phys. Rev. Lett. **88**, 022301 (2002).

[12] S. S. Adler *et al.* (PHENIX Collaboration), Phys. Rev. C **69**, 034910 (2004).

[13] C. Adler *et al.* (STAR Collaboration), Phys. Rev. Lett. **89**, 202301 (2002).

[14] J. Adams *et al.* (STAR Collaboration), Phys. Rev. Lett. **91**, 172302 (2003).

[15] B. B. Back *et al.* (PHOBOS Collaboration), Phys. Lett. **B578**, 297 (2004).

[16] I. Arsene *et al.* (BRAHMS Collaboration), Phys. Rev. Lett. **91**, 072305 (2003).

[17] C. Adler *et al.* (STAR Collaboration), Phys. Rev. Lett. **90**, 082302 (2003).

[18] F. Wang (STAR Collaboration), J. Phys. G **30**, S1299 (2004).

[19] S. S. Adler *et al.* (PHENIX Collaboration), Phys. Rev. C **71**, 051902(R) (2005).

[20] D. Magestro, talk given at *Hard Probes 2004*, available online at http://event-hardprobes04.web.cern.ch/event-hardprobes04/.

[21] P. Jacobs and X. N. Wang, Prog. Part. Nucl. Phys. **54**, 443 (2005).

[22] R. Baier, D. Schiff, and B. G. Zakharov, Annu. Rev. Nucl. Part. Sci. **50**, 37 (2000).

[23] A. Kovner and U. A. Wiedemann, in *Quark Gluon Plasma 3*, edited by R. C. Hwa and X.-N. Wang (World Scientific, Singapore, 2004).

[24] M. Gyulassy, I. Vitev, X. N. Wang, and B. W. Zhang, in *Quark Gluon Plasma 3*, edited by R. C. Hwa and X.-N. Wang (World Scientific, Singapore, 2004).

[25] C. A. Salgado, Mod. Phys. Lett. A **19**, 271 (2004).

[26] K. J. Eskola, H. Honkanen, C. A. Salgado, and U. A. Wiedemann, Nucl. Phys. **A747**, 511 (2005).

[27] X. N. Wang, Phys. Lett. **B579**, 299 (2004).

[28] M. Gyulassy, I. Vitev, and X. N. Wang, Phys. Rev. Lett. **86**, 2537 (2001).

[29] R. Baier, Nucl. Phys. **A715**, 209 (2003).

[30] A. Accardi *et al.*, in *CERN Yellow Report on Hard Probes in Heavy Ion Collisions at the LHC*, edited by U. A. Wiedemann (CERN, Geneva, 2004).

[31] A. Dainese, C. Loizides, and G. Paic, Eur. Phys. J. C **38**, 461 (2005).

[32] A. Drees, H. Feng, and J. Jia, Phys. Rev. C **71**, 034909 (2005).

[33] X. N. Wang, Phys. Rev. C **63**, 054902 (2001).

[34] S. S. Adler *et al.* (PHENIX Collaboration), Phys. Rev. C **69**, 034909 (2004).

[35] J. Adams *et al.* (STAR Collaboration), Phys. Rev. Lett. **92**, 112301 (2004).

[36] K. H. Ackermann *et al.* (STAR Collaboration), Phys. Rev. Lett. **86**, 402 (2001).

[37] K. Adcox *et al.* (PHENIX Collaboration), Phys. Rev. Lett. **89**, 212301 (2002).

[38] S. S. Adler *et al.* (PHENIX Collaboration), Phys. Rev. Lett. **91**, 182301 (2003).

[39] E. Schnedermann, J. Sollfrank, and U. Heinz, Phys. Rev. C **48**, 2462 (1993).

[40] P. Huovinen, P. F. Kolb, U. W. Heinz, P. V. Ruuskanen, and S. A. Voloshin, Phys. Lett. **B503**, 58 (2001).

[41] P. F. Kolb, U. W. Heinz, P. Huovinen, K. J. Eskola, and K. Tuominen, Nucl. Phys. **A696**, 197 (2001).

[42] D. Teaney, J. Lauret, and E. V. Shuryak, Phys. Rev. Lett. **86**, 4783 (2001).

[43] P. F. Kolb and U. Heinz, in *Quark Gluon Plasma 3*, edited by R. C. Hwa and X.-N. Wang (World Scientific, Singapore, 2004).

[44] T. Hirano and K. Tsuda, Phys. Rev. C **66**, 054905 (2002).

[45] F. Retiere and M. A. Lisa, Phys. Rev. C **70**, 044907 (2004).

[46] N. Armesto, C. A. Salgado, and U. A. Wiedemann, Phys. Rev. Lett. **93**, 242301 (2004, as suggested).

[47] J. Y. Ollitrault, Phys. Rev. D **46**, 229 (1992).

[48] N. Borghini, P. M. Dinh, and J. Y. Ollitrault, Phys. Rev. C **63**, 054906 (2001).

[49] T. Hirano and Y. Nara, Phys. Rev. C **68**, 064902 (2003).

[50] I. G. Bearden *et al.* (BRAHMS Collaboration), Phys. Rev. Lett. **94**, 162301 (2005).

[51] S. A. Voloshin, arXiv:nucl-th/0312065.

[52] C. A. Salgado and U. A. Wiedemann, Phys. Rev. Lett. **89**, 092303 (2002).

[53] B. Abbott, M. Bhattacharjee, D. Elvira, F. Nang, and H. Weerts (D0 Coll.), FERMILAB-PUB-97-242-E.

[54] A. Majumder and X. N. Wang, Phys. Rev. D **72**, 034007 (2005).

[55] A. Majumder and X. N. Wang, Phys. Rev. D **70**, 014007 (2004).

[56] D. Kharzeev, E. Levin, and L. McLerran, Nucl. Phys. **A748**, 627 (2005).

[57] J. Jalilian-Marian and Y. V. Kovchegov, Phys. Rev. D **70**, 114017 (2004); **71**, 079901(E) (2005).

[58] J. W. Qiu and I. Vitev, Phys. Rev. Lett. **93**, 262301 (2004).

[59] E. Wang and X. N. Wang, Phys. Rev. Lett. **89**, 162301 (2002).

[60] R. Baier, Y. L. Dokshitzer, A. J. Mueller, and D. Schiff, Phys. Rev. C **58**, 1706 (1998).

[61] R. Baier, Y. L. Dokshitzer, A. H. Mueller, and D. Schiff, J. High Energy Phys. 0109 (2001) 033.

[62] F. Arleo, J. High Energy Phys. 0211 (2002) 044.

[63] T. Hirano and Y. Nara, Phys. Rev. C **66**, 041901(R) (2002).

[64] T. Hirano and Y. Nara, Phys. Rev. C **69**, 034908 (2004).